Hydrothermal Synthesis of Hierarchical Nickel- or Cobalt-Based Carbonate Hydroxides for Supercapacitor Electrodes

Yaling Li, Pengcheng Li, Zhiqing Xin, Zhicheng Sun, Meijuan Cao and Luhai Li[*]

Beijing Engineering Research Center of Printed Electronics, Beijing Institute of Graphic Communication, Beijing 102600, PR China
[*]E-mail: liluhai@bigc.edu.cn

Nickel-, cobalt- and nickel-cobalt carbonate hydroxides were prepared with hydrothermal method and the crystal structure, thermal property and morphology were characterized. The electrochemical performance was also studied using the three-electrode method in 6M KOH electrolyte. Nickel carbonate hydroxide and nickel-cobalt carbonate hydroxide have fluffy and hierarchical structures and exhibit much higher specific capacity compared to the as-prepared cobalt carbonate hydroxide. The specific capacity of nickel carbonate hydroxide achieves up to 169.6 mA h g^{-1} and that of the nickel-cobalt carbonate hydroxide reveals 127.4 mA h g^{-1} at a current density of 1 A g^{-1}. The two kinds of carbonate hydroxides exhibit superior cycling stability and have great application prospect for supercapacitor electrodes.

1. INTRODUCTION

Supercapacitors have high power density, superior cycling stability and good security compared to traditional batteries. [1-2] Supercapacitor electrode materials as the crucial materials have been studied widely and generally fall into some categories such as carbon materials, [3-6] metal oxides, [7-9] metal hydroxides, [10-15] conductive polymers [16] and their hybridize composites. The major factors such as the conductivity, morphology, pore size distribution, specific surface area and surface functionalization are considered to be the most active ways to enhance the electrochemical performance. [1, 7] Hydrothermal method has unique advantage of controlling the morphology through self-assembled method and is facile to acquire hierarchical porous material with good electrochemical properties. In recent years, carbonate hydroxides have been reported such as nickel

carbonate hydroxide (NiCH), [17] nickel copper carbonate hydroxide (NiCuCH), [18] copper cobalt carbonate hydroxide (CuCoCH), [19] graphene oxide-induced nickel cobalt carbonate hydroxide (GO/NiCoCH), [20] cobalt carbonate hydroxide (CoCH) [21-22] nickel carbonate hydroxide/zeolitic inidazolate framework-8 (NiCH/ZIF-8). [23] These carbonate hydroxide materials exhibit good electrochemical properties due to the hydrophilic CO_3^{2-} ion in this material and thus improving good wettability with electrolyte. [19] Nickel based electrode materials such as nickel oxide (NiO) and nickel hydroxide ($Ni(OH)_2$) have been generally studied due to their high theoretical specific capacity. [24] Cobalt can affect the morphology and improve the conductivity of the electrode materials and thus enhance their electrochemical properties. [25-27] Therefore, cobalt maybe can enhance the electrochemical properties of nickel carbonate hydroxide.
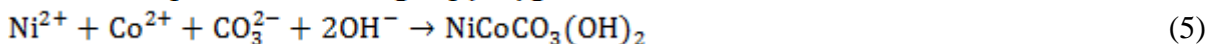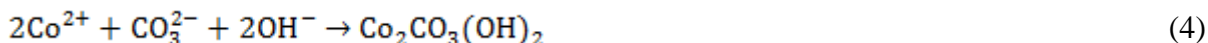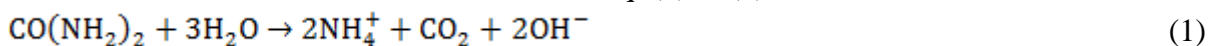
Here, we report a facile hydrothermal method to prepare porous metal carbonate hydroxides by using the nickel and/or cobalt salt and urea as raw materials by controlling the reaction temperature, reaction time and the urea dosage. The as-prepared products exhibit high specific capacity due to the fluffy and porous morphology. The NiCo CH electrode exhibits better cycling stability than the pure nickel or cobalt carbonate hydroxide electrode.

2. EXPERIMENTAL

2.1 Preparation of NiCH, CoCH and NiCoCH

All the chemical reagents were of analytical grade and used directly in the experiment. The nickel and/or cobalt carbonate hydroxides were prepared with hydrothermal method. Briefly, 0.008 mol $NiNO_3 \cdot 6H_2O$ or 0.008 mol $CoSO_4 \cdot 7H_2O$ and 0.02 mol urea were dissolved into 60 mL deionized water and transferred to a Teflon-lined stainless steel autoclave and maintained at 90°C for 14 hrs and then cooled down to the room temperature naturally. The precipitate was centrifuged and washed with water and ethanol several times. The result product was dried at 80 °C in a vacuum oven for 12 hrs and denoted as NiCH or CoCH, respectively. In the similar process, NiCoCH was prepared using 0.008 mol $NiNO_3 \cdot 6H_2O$, 0.008 mol $CoSO_4 \cdot 7H_2O$ and 0.04 mol urea as raw materials.

In the whole process, urea supplies both carbonate and hydroxyl anion under a hydrothermal condition and the reactions are listed as follows from Eq. (1) to (5). [18, 28-29]

$$CO(NH_2)_2 + 3H_2O \rightarrow 2NH_4^+ + CO_2 + 2OH^- \tag{1}$$

$$CO_2 + 2OH^- \rightarrow CO_3^{2-} + H_2O \tag{2}$$

$$2Ni^{2+} + CO_3^{2-} + 2OH^- \rightarrow Ni_2CO_3(OH)_2 \tag{3}$$

$$2Co^{2+} + CO_3^{2-} + 2OH^- \rightarrow Co_2CO_3(OH)_2 \tag{4}$$

$$Ni^{2+} + Co^{2+} + CO_3^{2-} + 2OH^- \rightarrow NiCoCO_3(OH)_2 \tag{5}$$

2.2 Characterization and electrochemical measurement

The as-prepared carbonate hydroxides were confirmed by thermogravimetric analysis (TG, Netzsch TG209F3) and X-ray diffraction (XRD, Rigaku Dmax/2200PC). The morphology was

measured by field emission scanning electron microscope (FESEM, Hitachi SU8020). The electrochemical measurements including cyclic voltammetry (CV), galvanostatic charge-discharge (GCD) and electrochemical impedance spectroscopy (EIS) were conducted on a potentiostat galvanostat (Metrohm, AUTOLAB PGSTAT302N) with three-electrode method using platinum plate as counter electrode and Hg/HgO electrode as reference electrode. The working electrode was prepared with mixing 80 wt% of as-prepared NiCH, CoCH or NiCoCH, 10 wt% of polyvinylidenefluoride (PVDF, HSV900, Arkema) and 10 wt% of acetylene black in N-methylpyrrolidone (NMP) and coating with the active area of 1×1 cm^2 onto the nickel foam. The electrode was dried and pressed under 10 MPa using a FW-4A tablet machine and the mass loading of the active material in each electrode is about 1.9 mg. Finally, the nickel carbonate hydroxide electrode was charged and discharged 1000 cycles at a current density of 10 A g^{-1} to evaluate its cyclic stability for practical application.

3. RESULTS AND DISCUSSION

3.1 Thermal analysis and crystal structure

TG and XRD measurements of the as-obtained materials were conducted to discuss the product validation including the formula and crystal structure, and the results are shown in Fig.1. Meanwhile, the products annealed at 400 °C under nitrogen and the residual samples measured after TG were characterized by XRD and the results are demonstrated in Fig.1.

In Fig.1a, there are three weight loss steps in the differential thermogravimetric (DTG) curve and the first two steps are caused by the lost of absorbed water and crystal water, respectively. If the molecular formula of the as-prepared nickel based material without crystal water is assumed to $Ni_2CO_3(OH)_2$, the third step is attributed to the decomposition based on Eq. (6).

$$Ni_2CO_3(OH)_2 \xrightarrow{\Delta} 2NiO + CO_2 + H_2O \tag{6}$$
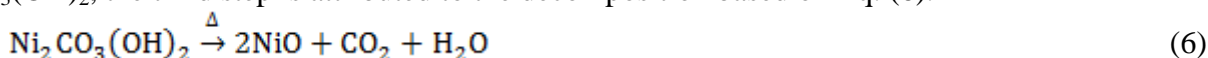
The decomposed product was confirmed by the XRD pattern in Fig.1b (2) and (3). As shown in Fig.1b (3), sharp and strong 2θ peaks at 37.3, 43.3, 62.9, 75.4 and 79.4° are good accordance with (111), (200), (220), (311) and (222) crystal planes of NiO (JCPDS No. 47-1049), respectively. The XRD pattern of nickel based material annealed at 400 °C under N_2 in Fig.1b (2) is also assigned to NiO with poor crystallinity. According to the Eq.6, the theoretical weight loss is calculated to be 29.3 %. While the weight loss between 200 °C and 400 °C of the TG curve in Fig.2a is 25.2 % and it should be 30.4 % except the physical absorbed water of 5.5 % and the crystal water of 11.5 %. The actual weight loss due to the removal of CO_2 and H_2O in Eq.6 is close to the theoretical weight loss, which suggest that the assumption is correct and the molecular formula is $Ni_2CO_3(OH)_2$. The second weight loss of 11.5 % caused by the loss of crystal water should be 12.1% excluding the physical absorbed water and so the molecular formula of as-obtained nickel based product could be $Ni_2CO_3(OH)_2 \cdot 1.6H_2O$. The decomposed process is shown in Eq. (7).

$$Ni_2CO_3(OH)_2 \cdot 1.6H_2O \xrightarrow{\Delta} 2NiO + CO_2 + 2.6H_2O \tag{7}$$
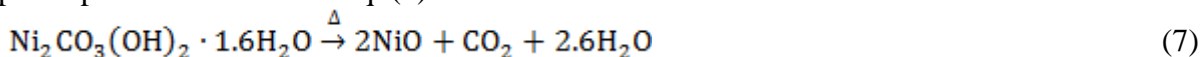
The theoretical residual weight of NiO is 62.2 %, while the actual residual weight of 57.8 % at 400 °C in Fig.1a should be 61.2 % excluding the physical absorbed water. The two values are very

close, which confirms the molecular formula of $Ni_2CO_3(OH)_2\cdot1.6H_2O$. The XRD pattern of the as-prepared nickel based product shown in Fig.1b (1) is assigned to $Ni_2(CO_3)(OH)_2$ (JCPDS No. 35-0501), while the intensity of the (110) and (120) planes are stronger compared to the standard card, which may be caused by the crystal water. [17]
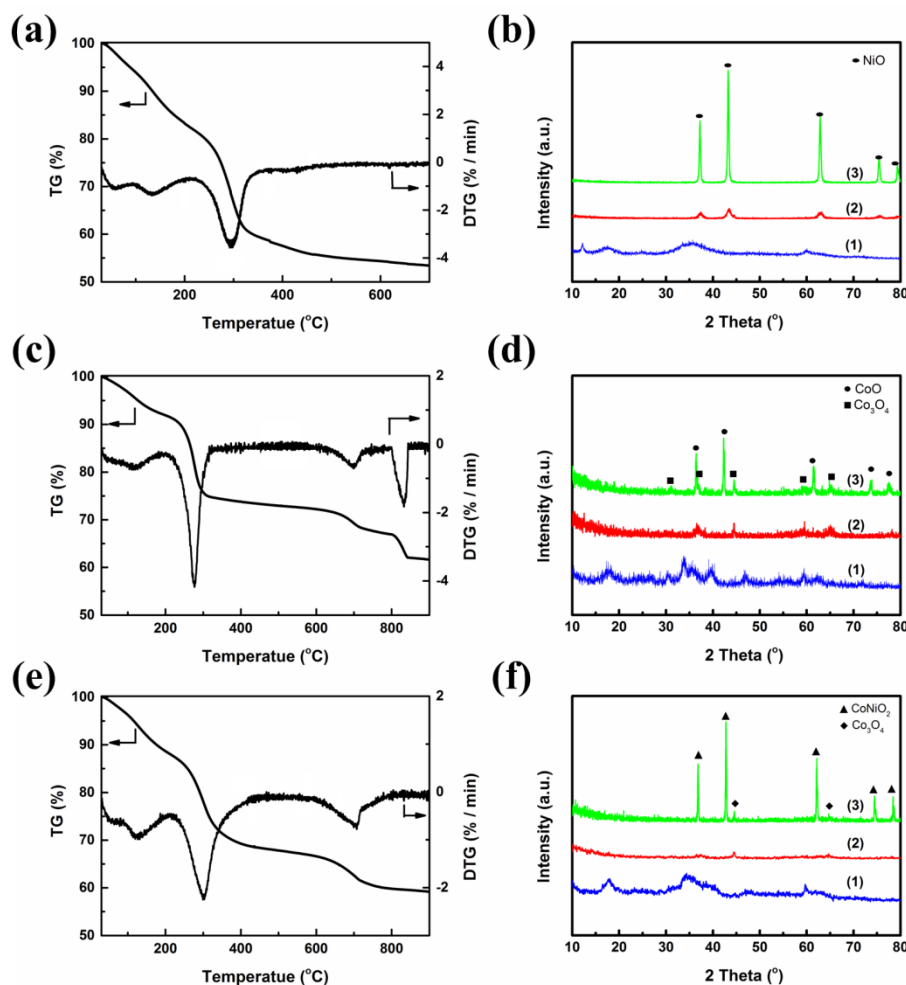

Figure 1. TG and DTG curves of (a) NiCH, (c) CoCH, (e) NiCoCH and XRD patterns of (b) NiCH (d) CoCH, (f) NiCoCH (In XRD figures, (1) as-prepared materials (2) the products annealed at 400°C in N_2 atmosphere (3) the residual sample measured after TG).

In Fig.1d (1), all the diffraction peaks are agreed with $Co_2(OH)_2CO_3$ (JCPDS No. 48-0083), which was accordance with the previous report. [30] The $Co_2(OH)_2CO_3$ decomposed to Co_3O_4 (JCPDS No. 43-1003) after calcinations at 400 °C in Fig.1d (2) and to the mixture of CoO (JCPDS No. 65-2902) and Co_3O_4 after calcinations at 900 °C in Fig.1d (3). The weight loss of CoCH between 200 °C and 450°C in Fig.1c should be related to the Eq.(8). The oxygen came from the residual air in the TG furnace.

$$3Co_2CO_3(OH)_2 + O_2 \xrightarrow{\Delta} 2Co_3O_4 + 3CO_2 + 3H_2O \tag{8}$$
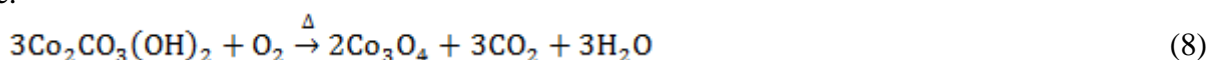
The theoretical weight loss is calculated to be 24.2%, and the practical weight loss of 21.3 % between 200 °C and 450 °C except the absorbed water and the crystal water is less than the theoretical

value because of the lack of oxygen in TG furnace. The two weight loss steps between 600 ^{o}C and 900°C are attributed to the transformation among the cobalt oxides and the final decomposed products are the mixture of CoO and Co_3O_4, which were demonstrated by the XRD pattern in Fig.1d (3).

The XRD pattern of NiCoCH is shown in Fig.1f (1) and that of the decomposed material corresponding to the second weight loss step is shown in Fig. 1f (2). The weight loss in TG curve between 550 ^{o}C and 900 ^{o}C in Fig.1e is attributed to the formation of $CoNiO_2$, which is demonstrated in the XRD pattern of the residual material calcined at 900 ^{o}C in Fig.1f (3). The final residual is composed of $CoNiO_2$ (JCPDS 10-0188) and Co_3O_4. [31] The DTG curve of NiCoCH has abroad decomposed peak between 200 ^{o}C and 450 ^{o}C in Fig.1e because the nickel and cobalt atoms coexist in NiCo CH.

3.2 Morphology

The SEM images of the as-prepared carbonate hydroxides are shown in Fig.2. As can be seen from Fig.2a and b, the fluffy NiCH microsphere with a diameter of about 1 μm was assembled with uniform ultrafine spicules. The fluffy structure makes favor of the permeability or wettability of the electrolyte into the active material by using the capillarity effect, resulting in excellent electrochemical properties. Obviously, the CoCH (Fig.2c) and NiCoCH (Fig.2d) products have larger size than the NiCH has. The flower-like CoCH sample was composed of regularly arranged bundles. The morphology of NiCH is similar with the previous work [17], while the amount of urea and the reaction temperature decreases and the energy consumption decreases greatly in our work. The morphology of CoCH is obviously different from the reported CoCH [32] and we found that the molar ratio of the cobalt salt to urea and the reaction temperature have great effect on the morphology. The porous structure and interconnected nanosheets in NiCoCH microsphere not only act as a reservoir to storage much more electrolyte ions but also facilate to ions or charges trasportation.
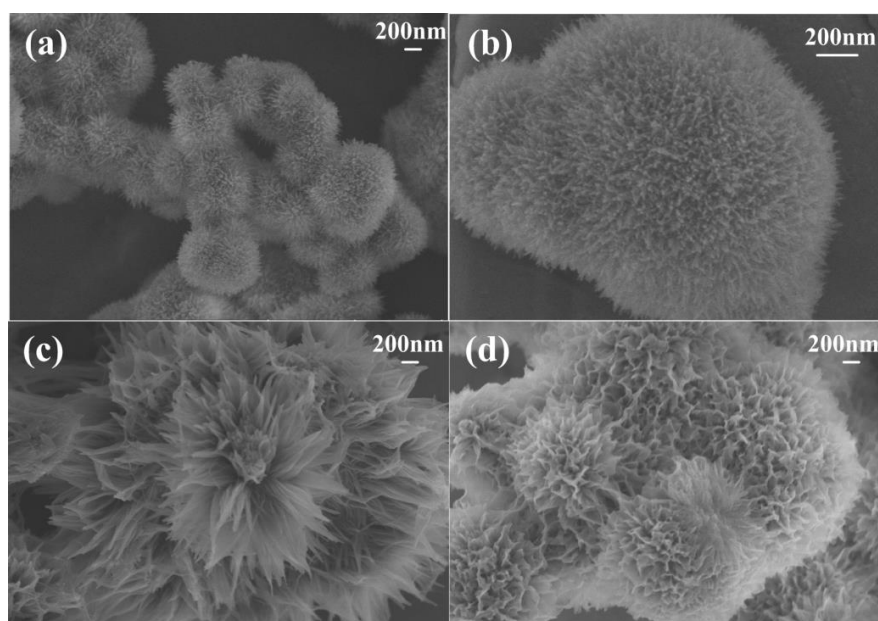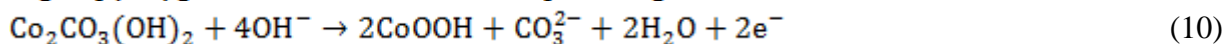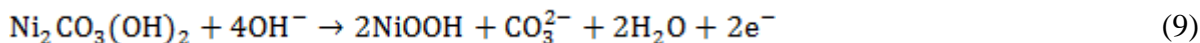

Figure 2. SEM images of (a, b) NiCH, (c) CoCH and (d) NiCoCH.

3.3 Electrochemical properties

Fig.3 shows the electrochemical performances of as-prepared carbonate hydroxide electrodes in 6M KOH electrolyte. The response current of the NiCH and NiCoCH electrodes is much larger than that of the CoCH electrode as shown in Fig.3a, revealing the higher charge storage. The anodic and cathodic peaks are obviously observed and the involved faradic reactions are based on Eqs. (9) and (10):

$$Ni_2CO_3(OH)_2 + 4OH^- \rightarrow 2NiOOH + CO_3^{2-} + 2H_2O + 2e^- \tag{9}$$

$$Co_2CO_3(OH)_2 + 4OH^- \rightarrow 2CoOOH + CO_3^{2-} + 2H_2O + 2e^- \tag{10}$$

The peak potential difference of 0.11 V for the NiCoCH electrode with peak potentials at 0.32 and 0.21 V is smaller than that for the NiCH electrode with peaks centered at about 0.4 and 0.26 V, which demonstrate that the NiCoCH electrode has superior reversibility and can be charged more easily. [33] The GCD curves at a current density of 1 A g^{-1} with the potential range from 0 to 0.5 V are shown in Fig.3b and the corresponding specific capacity (*C*sp) at different current densities is demonstrated in Fig.3c. The NiCH and NiCoCH exhibit superior electrochemical performance, which is accordance with the CV analysis. The NiCH electrode possesses a high specific capacity of 169.6 mA h g^{-1} at 1 A g^{-1}, while the NiCoCH electrode exhibit better specific capacity rate than the NiCH electrode and the specific capacity achieves 127.4 mA h g^{-1} at 1 A g^{-1} and still remains 97.2 mA h g^{-1} at 10 A g^{-1}, which may be explained by the improving conductivity with Co doping. The electrochemical performance of the NiCH and NiCoCH is superior to the previous reported cobalt hydroxide carbonate nanorods with the specific capacitance of 466 F g^{-1} at 1 A g^{-1}. [28]
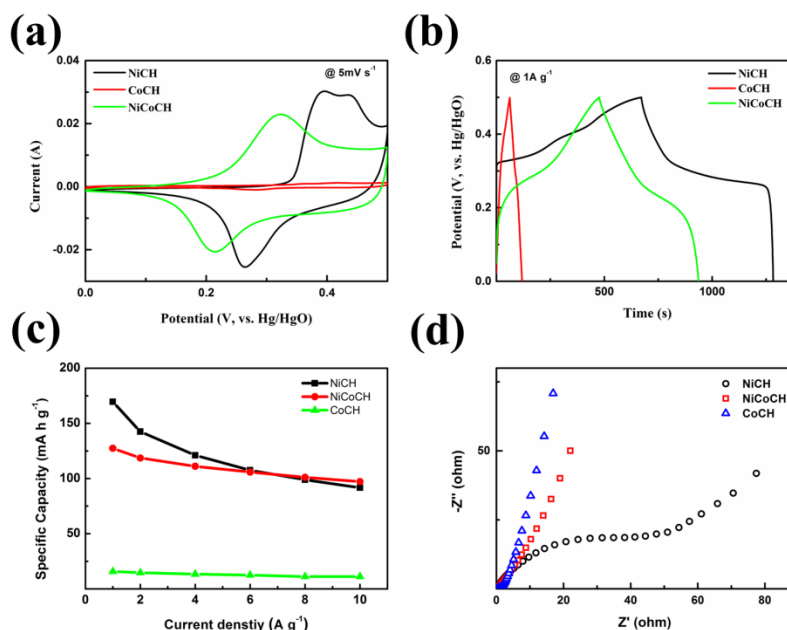

Figure 3. (a) CV curves at a scan rate of 5 mV s^{-1}, (b) GCD curves at a current density of 1 A g^{-1}, (c) Specific capacity versus current density and (d) Nyquist plots of NiCH, CoCH and NiCoCH.

The Nyquist plots of the NiCH, CoCH and NiCoCH electrodes are plotted in Fig.3d. Rs represent the electrolyte resistance, the intrinsic resistance and contact resistance of the electrode and it can be obtained with the X-intercept. The Rs values of as-prepared NiCH, CoCH and NiCoCH electrodes are 0.31, 0.39 and 0.33 Ω, respectively. There is no obvious semicircle denoting the charge transfer resistance (Rct) observed in the EIS spectra of the CoCH and NiCoCH electrodes, reflecting the superior conductivity. The NiCH electrode shows relative large charge transfer resistance explaining the inferior capacity rate mentioned above. In addition, the slope of straight line for the NiCH electrode is close to 45° indicating that the capacitive behavior is controlled by electrolyte ions diffusion process.

The CV curves of the NiCoCH electrode at different scan rates of 100, 50, 25, 10 and 5 mV s^{-1} are shown in Fig.4a and the GCD curves at various current densities of 10, 8, 6, 4, 2, 1 A g^{-1} are shown in Fig.4b. The oxidation peak shifts to the positive potential as the scan rate increases in Fig.4a due to the polarization of the electrode. The discharged time increases with the decreasing current density illustrated in Fig.4b. The specific capacity increases at low current density because of the full contact between the electrode and the electrolyte. Fig.4c shows the stability of the NiCH and NiCH electrodes charged and discharged continuously 1000 times at a current density of 10 A g^{-1} in 6M KOH electrolyte and the specific capacity increases at first and then gradually decreases. The maximum specific capacity of the NiCH electrode reaches up to 1.9 times of the initial capacity, and the capacity retention rate remains about 64 % of the maximum specific capacity and 118.8 % of the initial capacity after cycles. The specific capacity of the NiCoCH electrode increased obviously at first and then decreased gradually, which was about four times of the initial capacity. The obviously improved electrochemical performance at the initial cycling is related to the fluffy and hierarchical structures.
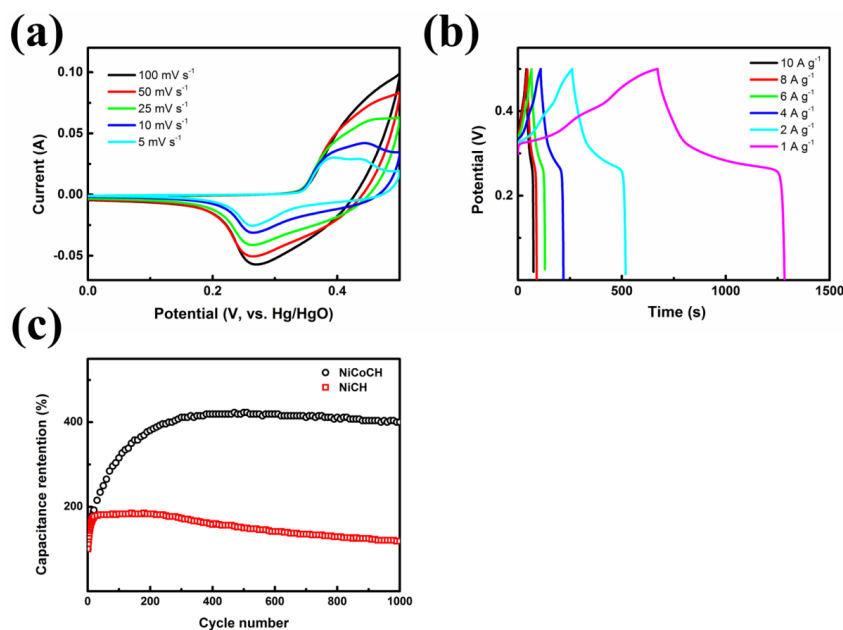

Figure 4. (a) CV curves at different scan rates of the NiCoCH electrode, (b) GCD curves at different current densities of the NiCoCH electrode and (c) cyclic stability at 10 A g^{-1} of the NiCH and NiCoCH electrodes.

4. CONCLUSIONS

In summary, we have synthesized three kinds of carbonate hydroxides i.e. nickel carbonate hydroxide, cobalt carbonate hydroxide and nickel-cobalt carbonate hydroxide with hydrothermal method using urea as the source of carbonate and hydroxyl ions. The nickel carbonate hydroxide and nickel-cobalt carbonate hydroxide exhibit superior electrochemical performance because of their fluffy and hierarchical structures. The nickel carbonate hydroxide electrode exhibits a maximum specific capacity of 169.6 mA h g^{-1} at 1 A g^{-1} and good cyclic stability. The nickel-cobalt carbonate hydroxide electrode achieves only 127.4 mA h g^{-1} at the same current density, while the nickel-cobalt carbonate hydroxide electrode exhibits superior cycling stability. These two kinds of carbonate hydroxides possess further application potential for supercapacitors.

References

1. G. Wang, L. Zhang and J. Zhang, *Chem. Soc. Rev.*, 41 (2012) 797.
2. D. Guo, L. Lai, A. Cao, H. Liu, S. Dou and J. Ma, *RSC Adv.*, 5 (2015) 55856.
3. L.L. Zhang and X.S. Zhao, *Chem. Soc. Rev.*, 38 (2009) 2520.
4. S. Bose, T. Kuila, A. K. Mishra, R. Rajasekar, N.H. Kim and J.H. Lee, *J. Mater. Chem.*, 22 (2012) 767.
5. Y.B. Tan and J.M. Lee, *J. Mater. Chem.* A, 1 (2013) 14814.
6. A.C. Ferrari, F. Bonaccorso, V. Fal'ko, K.S. Novoselov, S. Roche, P. Boggild, S. Borini, F.H. Koppens, V. Palermo, N. Pugno, J.A. Garrido, R. Sordan, A. Bianco, L. Ballerini, M. Prato, E. Lidorikis, J. Kivioja, C. Marinelli, T. Ryhanen, A. Morpurgo, J.N. Coleman, V. Nicolosi, L. Colombo, A. Fert, M. Garcia-Hernandez, A. Bachtold, G.F. Schneider, F. Guinea, C. Dekker, M. Barbone, Z. Sun, C. Galiotis, A.N. Grigorenko, G. Konstantatos, A. Kis, M. Katsnelson, L. Vandersypen, A. Loiseau, V. Morandi, D. Neumaier, E. Treossi, V. Pellegrini, M. Polini, A. Tredicucci, G. M. Williams, B.H. Hong, J.H. Ahn, J.M. Kim, H. Zirath, B.J. van Wees, H. van der Zant, L. Occhipinti, A. Di Matteo, I.A. Kinloch, T. Seyller, E. Quesnel, X. Feng, K. Teo, N. Rupesinghe, P. Hakonen, S.R. Neil, Q. Tannock, T. Lofwander and J. Kinaret, *Nanoscale*, 7 (2015) 4598.
7. M. Huang, F. Li, F. Dong, Y.X. Zhang and L.L. Zhang, *J. Mater. Chem.* A, 3 (2015) 21380.
8. W. Wei, X. Cui, W. Chen and D.G. Ivey, *Chem. Soc. Rev.*, 40 (2011) 1697.
9. M.S. Kolathodi and T.S. Natarajan, *Scripta Materialia*, 101 (2015) 84.
10. X. Long, Z. Wang, S. Xiao, Y. An and S. Yang, *Mater Today*, 19 (2016) 213.
11. S.S. Yang, M.J. Xie, Y. Shen, Y.Z. Wang, X.F. Guo and B. Shen, *Chinese Chem. Lett.*, 27 (2016) 507.
12. K. Ma, J. P. Cheng, F. Liu and X. Zhang, *J. Alloy Compd.*, 679 (2016) 277.

13. X.L. Guo, X.Y. Liu, X.D. Hao, S.J. Zhu, F. Dong, Z.Q. Wen and Y.X. Zhang, *Electrochim. Acta*, 194 (2016) 179.
14. J. Xing, S. Wu and K.Y.S. Ng, *RSC Adv.*, 5 (2015) 88780.
15. W. Ma, L. Wang, J. Xue and H. Cui, *J. Alloy Compd.*, 662 (2016) 315.
16. I. Shown, A. Ganguly, L.C. Chen and K.H. Chen, *Energy Sci. Eng.*, 3 (2015) 2.
17. Y. Jia, T. Luo, X.Y. Yu, J.H. Liu and X.J. Huang, *New J. Chem.*, 37 (2013) 534.
18. X. Zheng, Y. Ye, Q. Yang, B. Geng and X. Zhang, *Chem. Eng. J.*, 290 (2016) 353.
19. S. Liu, K.S. Hui, K.N. Hui, V.V. Jadhav, Q.X. Xia, J.M. Yun, Y.R. Cho, R.S. Mane and K.H. Kim, *Electrochim. Acta*, 188 (2016) 898.
20. J. Yang, C. Yu, X. Fan, C. Zhao and J. Qiu, *Adv. Funct. Mater.*, 25 (2015) 2109.
21. Z. Lu, W. Zhu, X. Lei, G.R. Williams, D. O'Hare, Z. Chang, X. Sun and X. Duan, *Nanoscale*, 4 (2012) 3640.
22. H. Xie, S. Tang, J. hu, S. Vongehr and X. Meng, *J. Mater. Chem.* A, 3 (2015) 18505.
23. Y. Gao, J. Wu, W. Zhang, Y. Tan, J. Gao, B. Tang and J. Zhao, *RSC Adv.*, 4 (2014) 36366.
24. B. Li, M. Zheng, H. Xue and H. Pang, *Inorg. Chem. Front.*, 3 (2016) 175.
25. G. Wang, G. Shao, J. Du, Y. Zhang and Z. Ma, *Mater. Chem. Phys.*, 138 (2013) 108.
26. J. Zhang, J.P. Cheng, M. Li, L. Liu, F. Liu and X.B. Zhang, *J. Electroanal. Chem.*, 743 (2015) 38.
27. Y.L. Li, L.H. Li, M.J. Cao, K. Dong, J.X. Wang, X.F. Zeng, J.F. Chen and L. Shao, *Int. J. Electrochem. Sci.*, 12 (2017) 3432.
28. T.M. Masikhwa, J.K. Dangbegnon, A. Bello, M.J. Madito, D. Momodu, F. Barzegar and N. Manyala, *J. Phys. Chem. Solids*, 94 (2016) 17.
29. S.D. Liu, K.S. Hui, K.N. Hui, V.V. Jadhav, Q.X. Xia, J.M. Yun, Y.R. Cho, R.S. Mane and K.H. Kim, *Electrochim. Acta*, 188 (2016) 898.
30. Y.H. Jin, L. Wang, Y.M. Shang, J. Gao, J.J. Li and X.M. He, *Electrochim. Acta*, 51 (2015) 109.
31. Y.Y. Yang, J.T. Sun, L.J. Yuan and K.L. Zhang, J. Wuhan Univ. (Nat. Sci. Ed.), 47 (2001) 660.
32. M. Yada, Y. Inoue, M. Koikawa, T. Torikai and T. Watari, *CrystEngComm.*, 14 (2012) 7374.
33. J. Xu, Y. Dong, J. Cao, B. Guo, W. Wang and Z. Chen, *Electrochim. Acta*, 114 (2013) 76.